AD-A193 708 DTIC FILE COPY

SECURITY CLASSIFICATION OF THIS PAGE (When Data Entered)

REPORT DOCUMENTATION PAGE

READ INSTRUCTIONS BEFORE COMPLETING FORM

1. REPORT NUMBER ARO 20498.6-MS	2. GOVT ACCESSION NO.
3. RECIPIENT'S CATALOG NUMBER	(2)
4. TITLE (and Subtitle) EROSION OF METALS EXPOSED TO HOT, DENSE GASES	5. TYPE OF REPORT & PERIOD COVERED Final 6/16/84 - 6/15/88
	6. PERFORMING ORG. REPORT NUMBER PSU
7. AUTHOR(s) Makoto Takeo	8. CONTRACT OR GRANT NUMBER(s) DAAG29-84-K-0080
9. PERFORMING ORGANIZATION NAME AND ADDRESS Department of Physics, Portland State University P.O.Box 751, Portland, Oregon 97207	10. PROGRAM ELEMENT, PROJECT, TASK AREA & WORK UNIT NUMBERS
11. CONTROLLING OFFICE NAME AND ADDRESS U. S. Army Research Office Post Office Box 12211 Research Triangle Park, NC 27709	12. REPORT DATE February, 1988 13. NUMBER OF PAGES 38
14. MONITORING AGENCY NAME & ADDRESS(if different from Controlling Office)	15. SECURITY CLASS. (of this report) 15a. DECLASSIFICATION/DOWNGRADING SCHEDULE

16. DISTRIBUTION STATEMENT (of this Report)

Aoproved for public release; distribution unlimited.

DTIC ELECTE APR 14 1988 S D

17. DISTRIBUTION STATEMENT (of the abstract entered in Block 20, if different from Report)

18. SUPPLEMENTARY NOTES

THE VIEW, OPINIONS, AND/OR FINDINGS CONTAINED IN THIS REPORT ARE THOSE OF THE AUTHOR(S) AND SHOULD NOT BE CONSTRUED AS AN OFFICIAL DEPARTMENT OF THE ARMY POSITION, POLICY, OR DECISION, UNLESS SO DESIGNATED BY OTHER DOCUMENTATION.

19. KEY WORDS (Continue on reverse side if necessary and identify by block number)

H in Metals
Device for Electron Diffraction

20. ABSTRACT (Continue on reverse side if necessary and identify by block number)

Metal foils were exposed in a ballistic compressor to a mixture of argon and hydrogen. Behavior of hydrogen is unpredictable.

When pure iron foil was exposed to a mixture of Ar with 16% H_2 (by volume) at 120 atmospheres and 1400° C about a

DD FORM 1 JAN 73 1473 EDITION OF 1 NOV 65 IS OBSOLETE

SECURITY CLASSIFICATION OF THIS PAGE (When Data Entered)

20 ABSTRACT

millisecond, precipitate particles of similar size (500 Å x 1000 Å) occured, oriented in the same direction in entanglement of matrix dislocations. The electron microdiffraction pattern indicates a distorted tetragonal structure, which seems to be $Fe_{16}H_2$. The diffractin pattern of the matrix shows a distorted bcc. A nitrogen-proton nuclear reaction confirmed the presence of hydrogen in the exposed foil and supports the predicted structure.

When pure chromium foil was exposed, streaks appeared in the electron diffraction pattern, possibly related to generation of lattice displacement waves.

Using a CCD video camera, a video digitizer, and a microcomputer, a device is constructed for analyzing electron diffraction patterns. This system can help to reduce the measurement time to one third when compared with conventional manual methods and produces results with better accuracy and less operator fatigue.

ARO 20798.6 MS

EROSION OF METALS EXPOSED TO HOT, DENSE GASES

FINAL REPORT

Makoto Takeo

February, 1988

U. S. ARMY RESEARCH OFFICE

Contract #DAAG29-84-K0080

Portland State University
Portland, Oregon 97201

Table of Contents

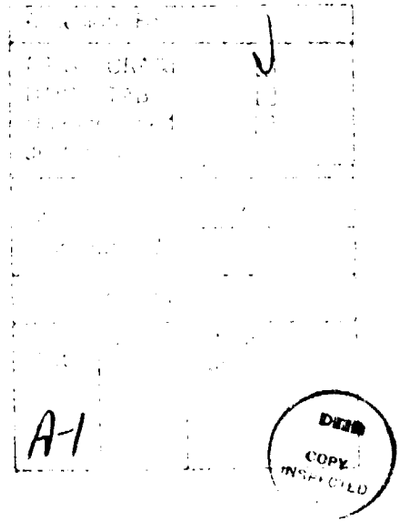

1. List of Appendixes

A1. Reprint of a publication. (Reference 1 in Bibliography.)
J. Dash, M. Takeo, A.R. Trzynka, J.M. Roush, A.M. Kasaaian, F.B. Brace, H. Takeo, and P.G. Weaver, "Effects of Hot, Dense Gases on the Structure and Composition of Materials", in Metallurgical Applications of Shock-wave and High-Strain-Rate Phenomena edited by L.E. Murr, K.P. Staudhammer, and M.A.Myers (Marcel Dekker Inc., New York and Base, 1986), pp. 1051-1069.

A2. Copy of a publication. (Reference 4 in Bibliography.)
A. Trzynka and M. Takeo, "Electronic device for the analysis of electron diffraction patterns", Rev. Sci. Instr., March (1988) in press.

2. Body of Report

a. Statement of the problem studied

The purpose of this research was to observe microscopic structural and chemical changes of metals due to exposure to a hot, dense gas of, mainly, argon containing hydrogen. The emphasis was placed on the study leading to understanding of the corrosion and erosion mechanisms when metals, such as iron and chromium, are under a hot, dense gaseous environment, in particular, of hydrogen.

A ballistic compressor has been used for obtaining hot, dense gases. A small metallic specimen was mounted on the piston head, so that it was directly exposed to a hot dense gas in the compressor. In order to avoid specimen melting, the peak condition of the compression had to be accordingly limited, though the compressor is capable of producing gases at more than 3×10^8 Pa and 6000 K for about a millisecond.

The dynamical and chemical effects of the hot, dense gases on the metals are likely to occur on or near the surface of the specimen. The surface structure changes were identified by an optical microscope and a scanning electron microscope (SEM) (1,A1). However, when a thin foil of iron (less than 1 micrometer thick) was exposed to a mixture of argon and hydrogen, it was observed that there were changes in d-spacings, typical of uniaxially ordered crystal structure. Then, it was realized that more interesting results might be obtained on microstructure changes in thin films (2,3). Thus, thin specimens were prepared by electrolytic thinning, alternate cold rolling in air and annealing in vacuum, or evaporation in vacuum. Then the effects of hot, dense gases were observed with a transmission electron microscope (TEM) to obtain micrographs and electron diffraction patterns. For the chemical effects an energy dispersive x-ray spectrometer (EDS) was used.

Hydrogen embrittlement of metals has been well known for a long time, and remains an unsolved problem. In the present research a ballistic compressor was used to generate a hot, dense hydrogen gas to which metals were exposed. The peak condition of the compressed gas lasts for about a millisecond and the cooling rate is very fast (10^5 K/sec). During the peak condition, metals mounted on the piston are exposed to the high density gas as well as soft shock waves, so that they are momentarily under a time-dependent strain field. Thus, exposed metals were subject to highly non-equilibrium conditions, and any changes made in the metals under such conditions were expected to be frozen due to the high cooling rate and could be observed at room temperature.

This research involves analysis of many electron diffraction patterns. The conventional method of analyzing electron diffraction patterns with a micrometer positioned microscope or with divider and scale is very tedious and time consuming, but the accuracy is usually poor. It is also a possible source of human bias. Thus, a new electronic device was constructed to improve the method of analysis in the sense of the time comsumption and accuracy (4,A2).

b. Summary of most important results

b.1 Formation of iron hydride in thin films of iron. (Reference 3.)

It is not easy to observe hydrogen in iron, probably because it is unstable (5). In fact, to our knowledge, iron hydride has never been observed at room temperature and at one atmosphere. Recently, however, an important result was obtained in this laboratory. Pure iron foils of about 30 micrometer thickness were exposed to a 40% hydrogen-argon mixture at the peak condition of about 470 atmospheres and 1700^{0} C. These samples were then analyzed for hydrogen concentration at room temperature using a gamma-emitting resonant nuclear reaction between nitrogen nuclei and protons (6). A 7.5 MeV ^{15}N beam was rastered over an area of about 0.3 cm^{2}. The analysis gave a value of $(1.8 \pm 0.7)\times10^{20}$ H atoms/cm^{3}, averaged over the rastered area. The location of H in the microstructure was determined by other methods, e.g., TEM as described below.

Iron foil (99.9985% Fe) 25 micrometer thick, supplied by AESAR, was alternately cold rolled and annealed at 700^{0} C in vacuum to achieve thickness less than 1 micrometer. It was exposed in the ballistic compressor to a mixture of Ar with 16% H_2 (by volume) at 1.2 X 10^{7} Pa and 1400^{0} C for about a millisecond. Micrographs were taken with a 200 kV scanning transmission electron microscope (STEM) at Lawrence Berkeley Laboratory (Fig.1). The unique feature is the appearence of a second phase (2,3). It appears in the form of particles of rhombic shape and all of similar size of about 500 Å X 1000 Å, oriented in the same direction in the entanglement of dislocations. The Fig.2a shows the electron microdiffraction pattern. With a theory, which is described later, the spots are indexed as illustrated in Fig.2b. In this figure, the indices carrying letter P belong to the particle and those with M to the matrix surrounding the particle. It was confirmed by measurements on a selected area diffraction pattern from the adjacent matrix that the pattern of spots carrying M is the same as that obtained from the matrix near the particle. Table 1 and 2 compare the experimental and theoretical values of the d-spacings and angles for the particle and the matrix (3). The agreement is excellent, indicating that the crystal structures of the particle and the matrix are respectively distorted tetragonal and bcc. By calculation we determined that the distortion is not due to a tilt of the electron beam against the pattern zone axis. The data in Table 2 was verified by measurements on a selected area diffraction pattern from the matrix alone.

It is unlikely that particles such as those in Fig.1 are caused by impurities because chemical analysis of these particles with a windowless EDS capable of detecting elements down to atomic number 6 showed that they have the same composition as the matrix. In addition, the cleanliness of the prepared sample has been judged by its clean electron diffraction pattern (absence of extra spots) taken prior to

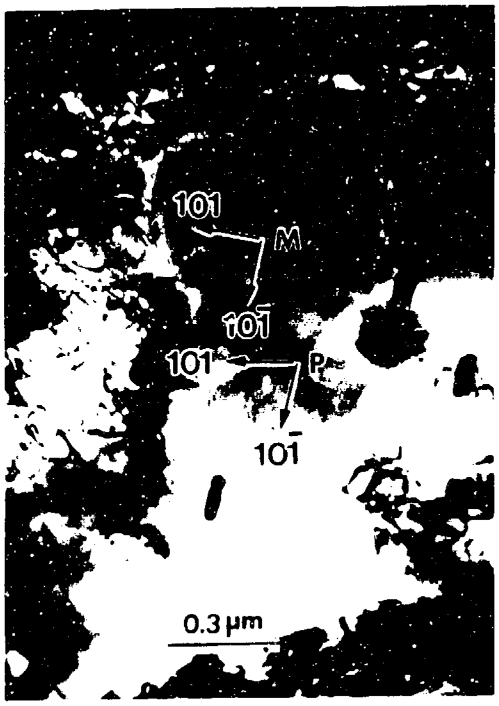

Fig.1 Micrograph of [illegible] exposed to 5 min fume of argon and 15% hydrogen. The approximate orientation relationship between the matri[illegible] (M) and the [illegible] (P) [illegible]

[010]$_M$ [illegible]

[101̄]$_M$ [illegible]

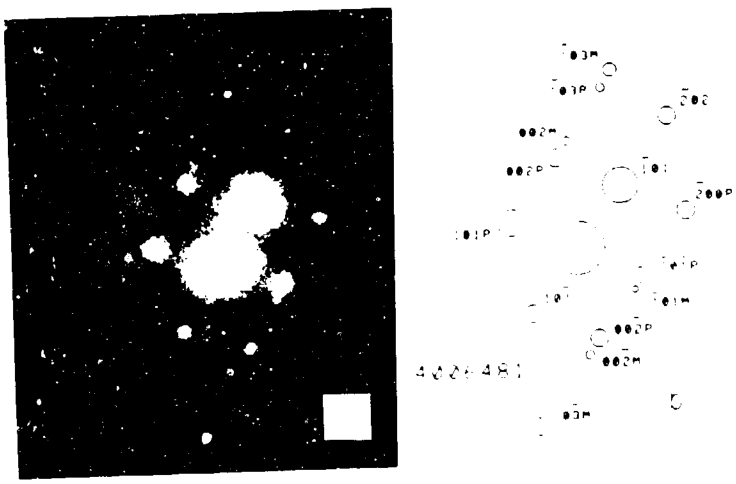

Fig.2a and b
a: The microdiffraction pattern [illegible] of a particle of Fig.1.
b: Schematic illustration of indexed spots. Symbol M or [illegible] stand for the matrix [illegible]

the exposure to [illegible] detected by the [illegible] [illegible] but, the [illegible] probably [illegible]

In general, hyd[illegible] at [illegible] well as at [illegible] [illegible] are [illegible] two types: [illegible] rounded [illegible]

Table 1

Angles and d-spacings of crystallographic planes of the particle (Angles are measured conterclockwise from $10\bar{1}$ in Fig.2a)

Index	Angles(degrees)		d-spacings(Å)	
	Exp.	Theor.	Exp.	Theor.
$10\bar{1}$	0	0	2.02	2.01
$00\bar{2}$	48.5	48.3	1.64	1.66
$\bar{1}01$	102.4	102.1	2.23	2.17
$\bar{2}00$	143.3	142.8	1.34	1.34
$\bar{1}01$	180.0	180.0	2.02	2.01
$\bar{2}02$	180.0	180.0	0.99	1.01
$\bar{1}03$	206.7	206.8	0.96	1.00
002	228.5	228.3	1.63	1.66
101	282.4	282.1	2.16	2.171

Table 2

Angles and d-spacings of crystallographic planes of the matrix surrounding the particle (Angles are measured counterclockwise from $10\bar{1}$ of the particle in Fig.2a)

Index	Angles(degrees)		d-spacings(Å)	
	Exp.	Theor.	Exp.	Theor.
$10\bar{3}$	24.0	24.2	0.86	0.86
$00\bar{2}$	41.0	41.3	1.40	1.38
$\bar{1}01$	87.7	86.8	2.20	2.08
$\bar{1}03$	204.0	204.2	0.86	0.86
002	221.0	221.3	1.42	1.38

and chromium. In fact, Myers and co-workers (8) observed this occupancy with deuterium atoms in alpha-iron. Thus, hydrogen may adopt the similar occupancy. A self-trapping site is created at the O-site by pushing two nearest neighboring iron atoms away, whereby O-site occupation is slightly stabilized (9). The distortion around the occupied O-site is strongly anisotropic, causing elongation along one direction (c axis). This elongation must be closely related to the size of the occupied hydrogen atom, i.e., the Fe-H bond length which is theoretically calculated by Chang to be 1.79 Å (10).

Since most of our efforts have been made on oure iron, the following discusasion is limited to the hydrogen-iron relationship. Fig.1, 2a and b seem to indicate some regularity, so that the inclusion of hydrogen in alpha-iron may be considered through a calculation using anisotropic elastic theory of Mori et. al. (11). These authors predict that elastic strain energy due to periodically arranged nitrogen atoms in iron is minimum for the arrangement of nitrogen atoms corresponding to $Fe_{16}N_2$. Considering the similar magnitude of the anisotropy of hydrogen and nitrogen in transition metals (12), it may be assumed that hydrogen would adopt the structure $Fe_{16}H_2$. The crystal structure is depicted in Fig.3 (13). Then the atomic percentage of hydrogen is 11.1% in the particle. This percentage is also supported by the value of the hydrogen content observed by the resonant nuclear reaction. In order to make the calculated d-spacings to agree with experimental ones in Table 2,

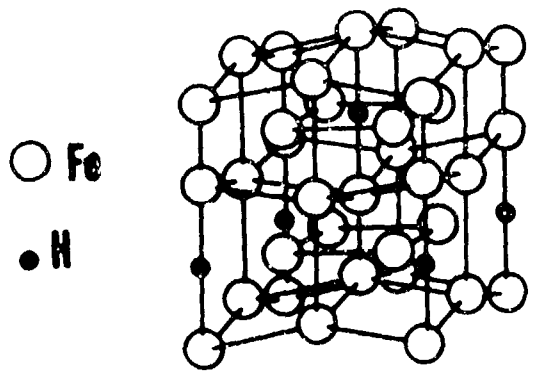

Fig.3 Structure of $Fe_{16}H_2$.

the Fe-H bond length was chosen to be 1.89 Å instead of Chang's value. For the angles, the best results were obtained if the angles between axes b and c, c and a, and a and b were respectively adjusted to

$$\text{alpha} = 90^{\circ}, \quad \text{beta} = 85.5^{\circ}, \quad \text{and} \quad \text{gamma} = 90^{\circ}$$

for the particle. Table 1 shows excellent agreement between the experimental and theoretical results. The matrix is also shown to be contracted by a strain 0.036 along the c axis, so that it is on the compression side and the particle is on the tension side of the distortion.

Since hydrogen atoms cause volume expansion of the lattice, they flow from the compression side to tension side of stressed specimen. Hydrogen diffusion is enhanced along dislocations. If a dislocation intersects a second phase particle, hydrogen atoms may easily transfer from the matrix to the particle when the matrix is on the compression side (14). Thus, hydrogen atoms are more likely present in the particle. In fact, the theoretical values in Table 2 are obtained for a distorted bcc lattice without hydrogen.

It is clear from the above discussion that, in Fig.2a, the c axis of the lattice, along which hydrogen atoms are trapped so that it is elongated, is perpendicular to the zone axis [010]. This means that the c axis is along the specimen surface. Then a stress due to the elongation, being along the surface, is easily transmitted in the specimen from the particles to the surrounding matrix, causing a strong correlation between the crystal orientations of the particle and the matrix. This is an effect of boundary conditions. This effect would differ if the specimen is very thin and the c axis is perpendicular to the surface. In this case, the elongation is not along the specimen surface and the correlation may hardly be established because of lack of a transmitted stress along the surface. Then the angular distortion of the lattice is also expected not to appear. An example for this case is given by Figs.4 and 5a and b, which were obtained from a specimen prepared by evaporation. Fig.4 shows appearance of particles of the same size as Fig.1. Fig.5a is a selected area diffraction pattern from the circular area of Fig.4. The measurement of d-spacings and angles on the pattern suggests that the lattices of the particles and the matrix are likely to without distortion. But it must be noted that unless the c axis is along the specimen surface there is, in general, a possibility of overlooking the elongation of the c axis in the determination of the crystal structure from the diffraction pattern, since the c axis is along the electron beam. Fig.5b shows that the zone axes are $[\bar{1}13]$ and $[02\bar{1}]$, respectively, for the particle and the matrix, so that the c axes are almost perpendicular to

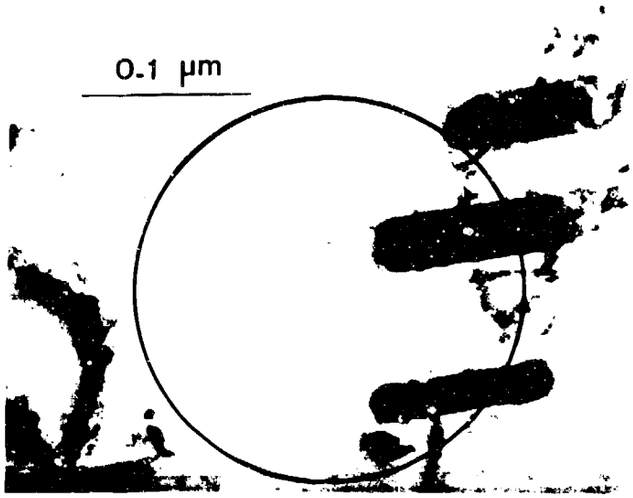

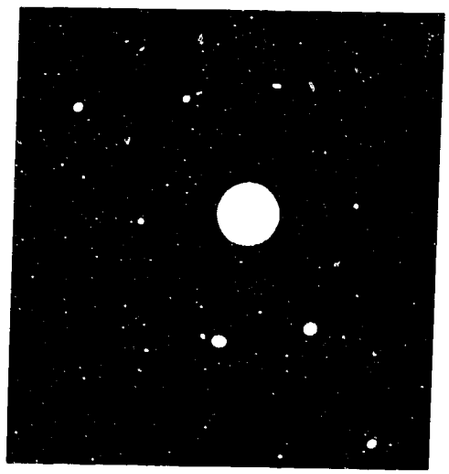

b

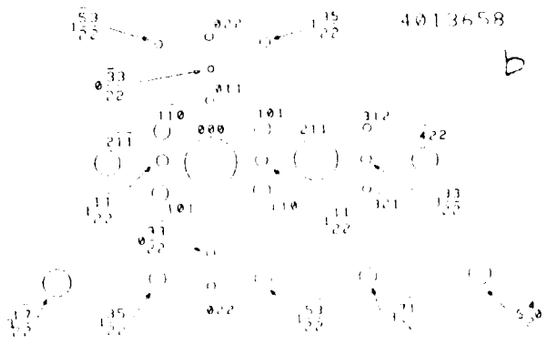

[illegible]

b.2 [illegible]

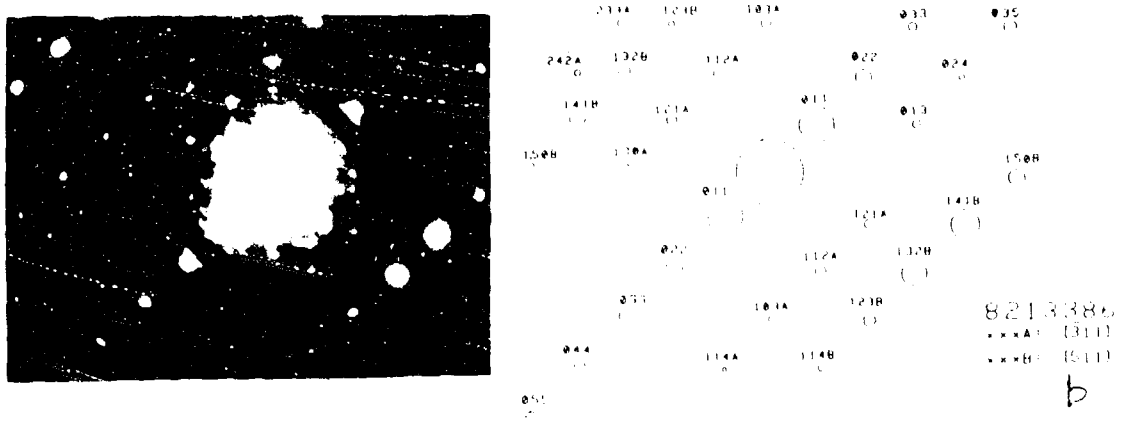
8213386

patterns seem to satisfy some conditions. Diffraction spots belonging to any zones appear near or at the intersections of the almost vertical and horizontal streaks of the [100] pattern (see figures). In other words, unless the spots can be near the intersections, the corresponding zones do not appear in the pattern. Such pattern were observed so far only with chromium exposed to hydrogen.

The relationship between the lattice displacement waves and any change in properties of metal is not clear. However, it may be speculated as follows. The nucleus of a hydrogen atom is a proton, which may be considered a point charge, and it creates a localized energy level energetically deep compared with the Fermi level. Each level is doubly degenerate because of electron spin and can hold two electrons, which may be from its own atom or supplied by the conduction band of the metal, making the hydrogen atom a negative ion. Then, hydrogen behaves as a larger sized particle in metals and reduces the number of conduction electrons which contribute to the metallic bond, causing the elastic properties to change. The deep lying level is characteristic of hydrogen (16). It is well known that hydrogen softens high purity iron at high temperatures (14).

b.3 Measurement of a diffusion coefficient of hydrogen in quartz at high temperatures (A1)

As described in A1, if hydrogen atoms or molecules can be trapped in a specimen with a good stability when exposed to a hot, dense hydrogen gas in a ballistic compressor, the diffusion coefficient of hydrogen (atomic or molecular) at the peak temperature can be determined by using the resonant proton-nitrogen nuclear reaction. (See Fig.4 and Eq.(7) of A1 and Reference 6). The value of the diffusion coefficient of hydrogen as a function of temerature is important in understanding the behavior of hydrogen in materials.

b.4. An electronic device for the analysis of electron diffraction pattern (A2)

A CCD-type video camera incorporating a silicon detector containing 510 light-sensitive cells horizontally and 492 light-sensitive cells vertically and a video digitizer with a spatial resolution of 512 x 480 pixels and a dynamic range of 8 bits per pixel are used together with a microcomputer to attain a desired accuracy of about 1% in determination of d-spacings.

The technique on noise reduction and image contrast in video image processing has been fully utilized in construction of the software for determining the locations of electron diffraction spots on photographic negatives of electron diffraction patterns.

The system can help reduce the measurement time to one third when compared with conventional manual methods and less operator fatigue.

c. List of publications and technical reports published

1. J. Dash, M. Takeo, A.R. Trzynka, J.M. Roush, A.M. Kasaaian, F.B. Brace, H. Takeo, and P.G. Weaver, "Effects of Hot, Dense Gases on the Structure and Composition of Materials", in Metallurgical Applications of Shock-wave and High-Strain-Rate Phenomena edited by L.E. Murr, K.P. Staudhammer, and M.A.Myers (Marcel Dekker Inc., New York and Base, 1986), pp. 1051-1069.

2. M. Takeo, J. Dash, A. Kasaaian, and A. Trzynka, "EFFECTS OF A MIXTURE OF HOT, DENSE H_2 AND AR ON THE STRUCTURE AND COMPOSITION OF IRON", Proceedings of the 9th International Conference on High Energy Rate Fabrication, Novosibirsk, USSR, Aug. (1986), pp. 121-125.

3. M. Takeo, J. Dash, A. Kasaaian, and A. Trzynka, "Effectsa of a Mixture of Hot, Dense H_2 and Ar on the Structure and Composition of Iron", AAPT/APS Joint Winter Meeting, San Francisco, California, January, 28-31, 1987.

4. A. Trzynka and M. Takeo, "Electronic device for the analysis of electron diffraction patterns", Rev. Sci. Instr., March (1988) in press.

5. M. Takeo, J. Dash, A. Kasaaian, A. Trzynka, and W.A. Lanford, "HYDROGEN IN IRON FOIL EXPOSED TO A HOT, DENSE GAS MIXTURE OF ARGON AND HYDROGEN", Scripta Met., submitted for publicatin.

d. List of scientific personnel supported by this project.

Makoto Takeo
John Dash
Andrew R. Trzynka
Arash M. Kasaaian
Yi Pan
Jeffrey Roush
B. Frederick Brace
Ching H. Tam
Elinor Trapp

3. Bibliography

1. J. Dash, M. Takeo, A.R. Trzynka, J.M. Rouch, A.M. Kasaaian, F.B. Brace, H. Takeo, and P.G. Weaver in Metallugical Applications of Shock-Wave and High-Strain-Rate Phenomena edited by L.E. Murr, K.P. Staudhammer, and M.A. Myers (Marcel Dekker Inc., New York and Basel, 1986) pp.1051-1069.
2. M. Takeo, J. Dash, A. Kasssian, and A. Trzynka, Proceedings of the 9th International Conference on High Energy Rate Fabrication, p.121, Novosibirsk, USSR, Aug. (1986).
3. M. Takeo, J. Dash, A. Kasaaian, A. Trzynka, and W.A. Lanford, Scripta Met., submitted for publication.
4. A. Trzynka and M. Takeo, Rev. Sci. Instr., March (1988) in press.
5. V.E. Antonov, I.T. Belash, V.F. Degtyareva, E.G. Ponyatovskii, and V.I. Shiryaev, Sov. Phys. Dokl. 25, 490 (1980).
6. W.A. Lanford and M.J.Rand, J. Appl. Phys. 49, 2473 (1978).
7. V.A. Somenkov and S.S. Chil'stein, Progress in Materials Science 24, 267 (1980).
8. S.M. Myers, S.T. Picraux, and R.E. Stoltz, J. Appl. Phy. 50, 5710 (1979).
9. Yuh Fukai, Jpn J. Appl. Phys. 22, 207 (1983).

10. Roger Chang, Scripta Met. 19, 1221 (1985).
11. T. Mori, P.C. Cheng, M. Kato, and T. Mura, Acta Metall. 26, 1435 (1978); Toshio Mura, Micromechanics of defects in solids (Martins Nijoff Publishers, The Hague, The Netherlands, 1982), pp.142-143.
12. Hidehiko Sugimoto and Yuh Fukai, Phys. Rev. B22, 670 (1980).
13. P. Ferguson, V. Dahman, and K.H. Westmacoff, Scripta Met. 18, 57 (1984).
14. John P. Hirth, Met. Trans. A 11A, 861 (1980)
15. Goro Honjo, Shiro Kodera, and Norihisa Kitamura, J. Phys. Soc. Japan 19, 351 (1964).
16. A.C. Switendick, Solid State Commun. 8, 1463 (1970); C.D. Gelett, H. Ehrenreich, and J.A. Weiss, Phys. Rev. B17, 1940 (1978); A.R. Williams, J. Kuebler, and C.D. Gelatt, Phys. Rev. B19, 6094 (1979); J.K. Nørskov, Phys. Rev. B26, 2875 (1982).

4. Appendixes

A1 and A2 follow.

Metallurgical Applications of Shock-Wave and High-Strain-Rate Phenomena

Edited by

Lawrence E. Murr
Oregon Graduate Center
Beaverton, Oregon

Karl P. Staudhammer
Los Alamos National Laboratory
Los Alamos, New Mexico

Marc A. Meyers
New Mexico Institute of
Mining and Technology
Socorro, New Mexico

MARCEL DEKKER, INC. New York and Basel

61

Effects of Hot, Dense Gases on the Structure and Composition of Materials

J. DASH, M. TAKEO, A. R. TRZYNKA, J. M. ROUSH, A. M. KASAAIAN, F. B. BRACE, H. TAKEO, and P. C. WEAVER[+]

Department of Physics
Portland State University
Portland, Oregon 97207

[+]Department of Physics
State University of New York at Albany
Albany, New York 12222

A free-piston type ballistic compressor capable of producing gases at temperatures as high as 600 K and pressures as high as 3000 atmospheres for about half a millisecond has been used to study effects on materials. The effects of the hot, dense gases were observed with a scanning electron microscope, an energy dispersive spectrometer, and a transmission electron microscope. The typical results are changes of alpha quartz to beta-crystobalite or melanophlogite, depending on impurities, on exposure to hot, dense argon. When stainless steel was exposed to the gas, the Cr/Fe ratio changed by about 30% on the exposed surface. On the other hand, when iron was exposed to a hot, dense hydrogen-argon mixture, it was subjected to changed in d spacings, typical of uniaxially ordered crystal structure.

I. INTRODUCTION

When materials are exposed to reactive gases, corrosion or erosion occurs. If the temperature and pressure of the gases change rapidly with time

there may be thermal and mechanical stresses over the surface. If the cooling rate is very rapid, structures which appeared at elevated temperatures may be retained at ambient. If hydrogen molecules are present, they may easily diffuse into the materials and modify the physical properties.

A ballistic compressor is a unique apparatus to produce hot, dense gases. The peak density can be comparable to that of a liquid. It allows observations of chemical reactions, which occur at high temperatures and pressures, and microstructure changes in materials exposed to hot, dense gases. The exposure is very short, but can be easily repeated on the same sample at the same conditions, and the cooling rate is as fast as about 10^{5}°C/sec.

When materials are mounted on the piston of the compressor, they will be exposed to hot, dense gases, and then transferred to various testing and examining apparatus. The apparatus involved in this report includes a scanning electron microscope (SEM), an energy dispersive X-ray spectrometer (EDS), and a transmission electron microscope (TEM). For observation of hydrogen content, the nuclear reaction analysis technique is used [1]. Since some unusual conditions of high gas density, high gas temperature, and high cooling rate are expected with a ballistic compressor, some new observations may be possible, though the identification is usually not easy.

This paper is intended to introduce recent results obtained with our ballistic compressor on effects on materials exposed to hot, dense gases. Materials involved were quartz, stainless steel, an amorphous iron alloy, and pure iron. The emphasis of the analysis was on changes in crystal structure, microstructure, and chemical composition. The choice of quartz has implications of geological applications of a ballistic compressor. The type of gas used is argon, since it is a typical inert gas which hardly reacts with materials under the conditions obtainable with the present ballistic compressor. About ten to twenty-five percent volume of hydrogen was added to the argon to observe the effect of hydrogen on materials.

II. DESCRIPTION AND OPERATION OF THE PSU BALLISTIC COMPRESSOR

The ballistic compressor at Portland State University is a modification of the original structure, which has already been fully described elsewhere [2]. The following is therefore limited to a brief description of the present device.

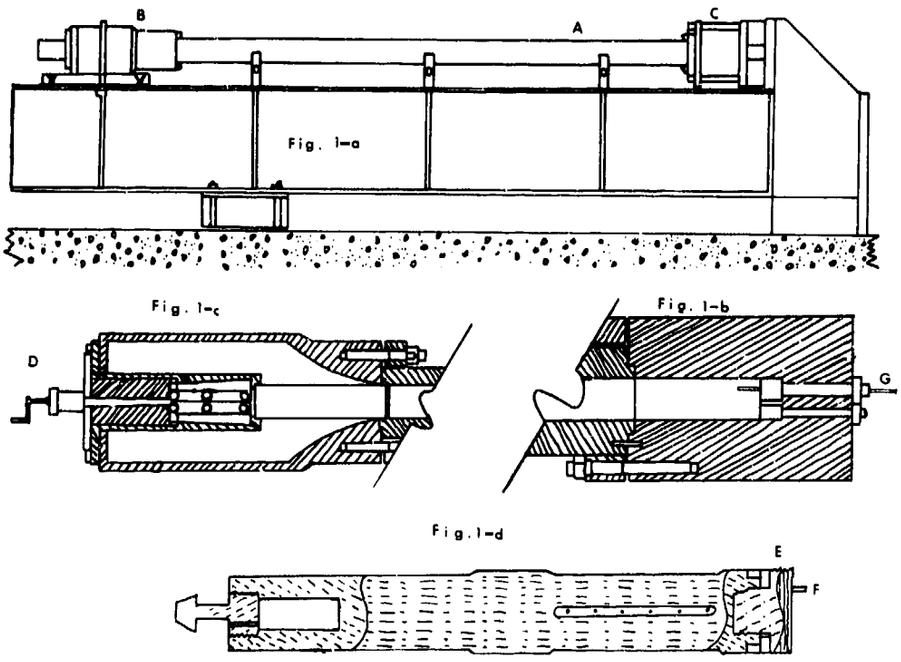

FIG. 1 *Diagrams of PSU ballistic compressor and the piston.*

As shown in Fig. 1, the compressor consists of a horizontally-mounted 2.90m long, 5.72cm inner diameter tube (A) attached on one end to the driving gas reservoir (B) and on the other to the high pressure head (C). With a 52.6cm long, 9.63kg piston in prefiring position, the volume of the driving gas reservoir is 10.57 liters, and the volume of the test gas chamber is 7.5 liters. The maximum possible stroke is 2.77m.

The high pressure head (Fig. 1-b) is made from ARMCO 17-4 PH stainless steel 25 cm in outside diameter, which is able to withstand a gas pressure of 6000 atmospheres. The driving gas reservoir (Fig. 1-c) contains the piston holding and release mechanism. In the prefiring position, the tail of the piston is engaged in the mechanism, which opens and pushes the piston slightly forward at firing by cranking the handle (D).

The piston is shown in Fig. 1-d. The piston head (E) has a diameter of .05mm less than the bore of the tube, and is made from the same material as the high pressure head. A short piece of 2-mm-diam steel rod (F), which has a screwed clamp at one end to hold a specimen, is attached to the front of the piston head.

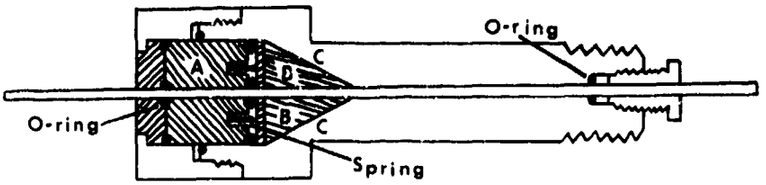

FIG. 2 *Mechanism for measuring the minimum volume of the compressed gas, which is positioned at Fig. 1-b (G).*

Figure 2 shows the mechanism of measuring the minimum volume of the compressed gas. It is a 15cm long sliding rod of 2mm in diameter and is mounted on the end wall of the high pressure head (Fig. 1-b (G)). The rod will move when the piston pushes it on one end. The other end appears outside the compressor and its displacement can be measured from the outside. The mechansm has a good pressure seal and the rod does not move if the force on it is only due to the gas pressure. It works as follows. The gas pressure pushes the steel block A, which in turn pushes three steel blocks B surrounding the rod. The blocks were cut from a cone. The three blocks sit on the shoulder C and if B's are pushed, they slide along the shoulder and push the rod, introducing a large enough frictional force on the rod.

A PCB Piezotronics Model 105A pressure transducer is mounted at an end of the side wall of the high pressure head. The output of the pressure transducer is recorded on an oscilloscope (Tektronix RM35A) with a polaroid camera. The peak pressure at each firing can thus be easily read on the oscillogram, but the gas temperature is found by using a computer program as described in detail elsewhere [2,3]. The program is to solve the equation of motion for the piston, with allowance for heat loss of the test gas by conduction through the compressor wall and gas leakage through the piston gap, and with the assumption of thermal equilibrium in both test and driving gases at any time during the compression and expansion of the gas systems.

A simple examination of the gas leakage can be made by observing the pressure profile at the instant of maximum radiation intensity from the compressed gas [4]. The leakage rate of the test gas in the compressor may be as large as 10 moles/sec near the peak pressure. If the piston gap is made small in order to reduce the leakage, the mechanical friction becomes very large and unpredictable since the driving force is limited, thus destroying the reproducibility of gas compression. If the gap is as

TABLE 1 *List of symbols used in Section II.*

a:	van der Waal's "a" constant, T-dependent
b:	van der Waal's "b" constant, T-dependent
F:	frictional force against the piston
L:	length of the piston
m:	mass of the piston
m_a:	molecular weight of the leaking gas
n:	the total number of moles of the compressed gas
dn:	number of moles of the leaking gas in dt
n_r:	the total number of moles of the driving (reservoir) gas
P,P_r:	pressure of the compressed, driving gas, respectively
q:	heat flow to the compressed gas in dt
δq_ℓ:	heat flow to the leaking gas in dt
R:	gas constant
r_o:	radius of the cylinder bore
r_p:	radius of the piston
T:	absolute temperature
t:	time
U,U_r:	internal energy of the compressed, driving gas, respectively
U_ℓ:	internal energy carried by the leaking gas from the compressed to the driving gas
$U_{r\ell}$:	internal energy carried by the leaking gas from the driving to the compressed gas
V,V_r:	volume of the compressed, driving gas, respectively
v:	velocity of the piston
x:	position of the piston measured from the prefiring position
η:	viscosity of the leaking gas
ρ:	density of the leaking gas

large as that of the present compressor, the piston is full floating inside the horizontal cylinder bore. Thus, the force on the piston due to the leaking viscous gas is solely the frictional force against the motion of the piston. Then the frictional force is given by

$$F = \pi r_o(r_o-r_p)/(P-P_r)+2\pi\eta vLr_o/(r_o-r_p). \quad (1)$$

(Symbols are explained in Table 1.)
The piston gap, $r_o - r_p$, is small, so that the first term can be neglected and the frictional force becomes proportional to the velocity of the piston. But the proportionality changes because the viscosity depends on temperature.

At the temperature attained in the ballistic compressor, the majority of gas molecules are in the electronic ground state. Therefore, it is justified to use the van der Waals' equation of state

$$(P+a/V^2) \cdot (V-b) = n \cdot R \cdot T \qquad (2)$$

for the gas systems, where constants a and b depend on temperature T.

The equation of motion for the piston is conveniently written in the form of an energy equation. For a time interval dt, the piston makes a displacement of dx. Then, the energy changes satisfy

$$mvdv = \delta q + \delta q_{\ell} - dU - dU_r - Fdx, \qquad (3)$$

where dU is the internal energy change of the test gas during dt due to a heat flow δq into the gas, due to the work on the piston and due to work $PVn^{-1}dn$ which causes dn moles of leaking gas to flow, and due to gas leakage which carries away a part of the internal energy, dU_{ℓ}. From the first law of thermodynamics,

$$dU = \delta q - PdV - PVn^{-1}dn - dU_{\ell} \qquad (4)$$

Similarly for the reservoir gas, for which an adiabatic process can be assumed,

$$dU_r = -P_r dV_r + P_r V_r n_r^{-1} dn + dU_{\ell r} \qquad (5)$$

The rate at which gas leaks through the piston gap is governed by the pressure difference between the test and driving gases. It is given by

$$\frac{dn}{dt} = \pi P (m_a)^{-1} r_o (r_o - r_p) \cdot \left[\frac{P-P_r}{8\eta L} (r_o - r_p)^2 + v\right]. \qquad (6)$$

The gas leaks from the reservoir to the test gas system at the beginning of the first stroke, but the direction is reversed in the course of compression. Equation (6) may be tested by finding the time lag between the pressure peak and the light output peak of the compressed gas [4].

The heat flow δq into the test gas is obtained by solving the well-known equation of thermal conduction applied to the compresser walls, by assuming that the gas systems are uniformly at their respective temperatures, and that the heat flow at the boundary is proportional to the difference of the temperatures of the gas and the inner surface of the walls. The proportionality constant is adjustable in the computation. Another adjustable parameter is the piston gap. At each firing, the

minimum volume of the test gas is measured by the mechanism Fig. 2. By assigning various values to the two adjustable parameters, the computer program is run until the computed minimum volume and peak pressure agree with observed ones. Then, the gas temperature profile as a function of time and the density in the test gas system are found. Usually a few trial runs on the computer are good enough to uniquely determine the thermodynamic conditions of the gas systems.

A test of the accuracy of the computed temperature was made at the melting point of tungsten [5]. There was a discrepancy of about 3%. The program has been used with the Naval Ordnance Laboratory ballistic compressor at the University of Florida to determine the equation of state of uranium hexafluorid, UF_6. The results of measurements of van der Waals' constants are accurate to about 10%. The compressor is capable of producing gases at temperatures of as high as 6000 K for about a millisecond. In the present observations, however, it is limited to about 2000 K in order to avoid losing samples by melting or evaporation.

III. EXPERIMENTAL PROCEDURE

Samples are mounted on the piston head by means of a pin with a screwed slot (Fig. 1-d (F)), so that they are directly exposed to the hot, dense gas during firing. In order to reasonably maximize the effects of hot, dense gases, the samples to be tested are made small to reduce the heat capacity and thin to increase the relative contact area with the gas. The mounting mechanism (Fig. 1-d (F)) seems to adequately reduce heat conduction without losing the security of mounting.

After exposure to hot, dense gases, samples were examined for changes in microstructure, crystal structure, and chemical composition under a TEM (Hitachi 125 kV or 1.5 MV TEM at Lawrence Berkeley Laboratory), a SEM (ISISS40), and/or an EDS (EDAX). Sample thickness was limited to about 0.2μm for the 125 kV TEM, but thicknesses of several μm could be studied with the 1.5 MV TEM.

The quartz specimens studied were obtained from high-frequency crystal oscillators (about 30 Mc/s) used in communication. The thickness was about 0.13 mm. Tapered samples of quartz were produced by breaking the oscillator crystals before mounting in the ballistic compressor. Thin areas near the fractured edges were sufficiently thin for TEM study. On the other hand, the stainless steel (Fe18%Cr12%Ni) used was prepared by rolling to about 30μm thickenss and annealing in a vacuum 1 hour at

1200°C. After this it was thinned electrolytically to produce regions as thin as 0.1μm for TEM study. This material is the same one as used by one of the present authors in investigations of the martensitic transformation [6]. The amorphous iron ($Fe_{78}B_{13}Si_9$)(30μm thick) was supplied by Sony, Sendai, Japan. Iron (50μm thick), which was of MARZ grade supplied by Material Research Corporation, was also used. It was reduced to about 1μm thickness by alternate rolling and annealing. The annealing was done in vacuum at 900°C for about 4 hours, and at the last stage of rolling the sample was sandwiched between copper foil. For mounting it on the piston, a folding molybdenum grid was used to hold the 1μm sample in position.

The type of gas used in this report is argon, pure or mixed with a known amount of hydrogen. The mixing was done in the test gas chamber in front of the piston in the firing position just before firing. The driving gas was always pure argon. Before the final process of firing, the ballistic compressor was flushed three or four times with argon to avoid any contamination of air, and in the final process enough time was given for the filled gas to reach room temperature.

IV. RESULTS AND DISCUSSION

Observations have been made on quartz, stainless steel, amorphous iron, and pure iron with our ballistic compressor using argon gas, sometimes mixed with hydrogen. Quartz was chosen as an example of geological applications in observations of effects on rocks, because quartz has various modifications of crystal structure, which may change from one to another under the thermodynamical conditions attainable with the ballistic compressor. Hydrogen gas is added for the purpose of observation of hydrogen behavior in metals, which might be related to hydrogen embrittlement.

With the aid of electron diffraction analysis, the crystal structure of the control quartz was found to be that of alpha-quartz (Fig. 3a). On exposure to argon gas at 790 atmospheres and 2800 K, the quartz changed to beta-crystobalite (Fig. 3b). This change was observed at places of the exposed quartz, where the sample was thin enough for electron diffraction analysis under a TEM (Hitachi 125 V). Such locations were found only at tapered edges of the exposed crystal.

Depending on impurities, quartz has various modifications in crystal structure. If the impurities are (carbon + hydrogen + sulfur), the modification has a structure called malanophlogite [7]. When a quartz

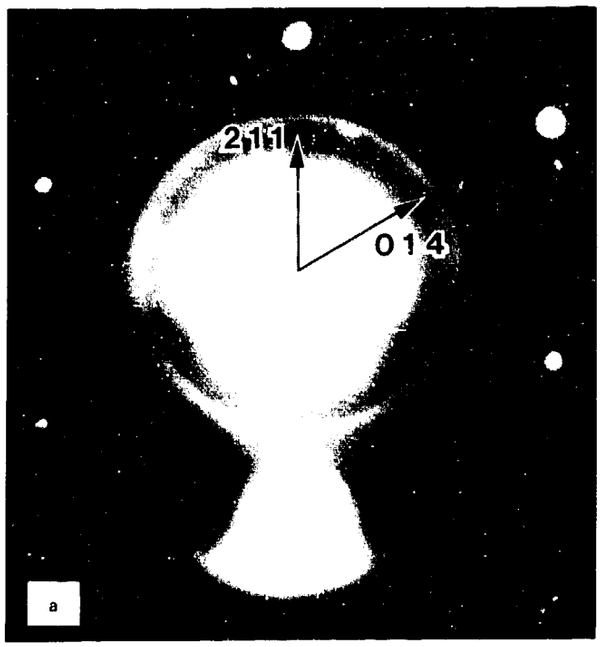

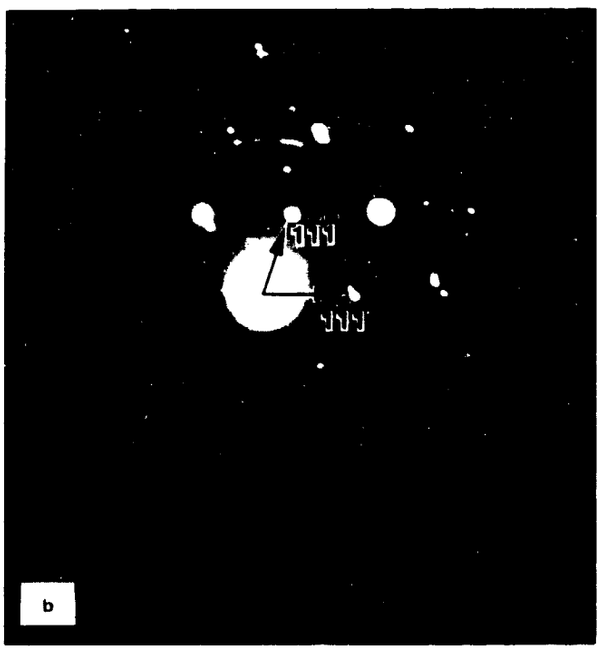

FIG. 3 *Electron diffraction patterns of quartz. (Rings are due to a reference gold foil.) (a) Unexposed (Control), (b) Exposed to argon gas at 790 atmospheres and 2800 K (beta-cristobalite), (c) Exposed to argon gas at 830 atmospheres and 2200 K (melanophlogite).*

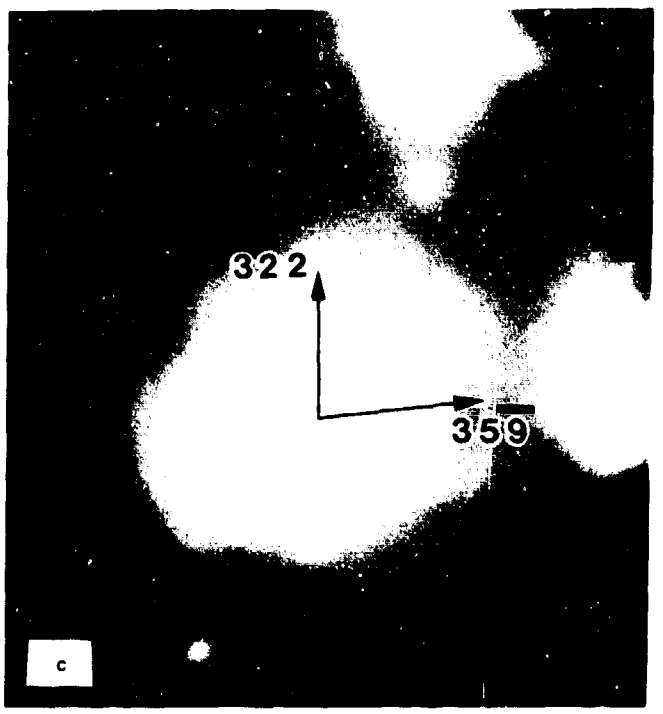

FIG. 3 *Continued.*

crystal, whose control was again alpha-quartz, was exposed to a hot, dense argon (830 atmospheres 2200 K), it turned to a melanophlogite structure (Fig. 3c, taken by a 1.5 MV Berkeley TEM). The impurities for the change of the crystal structure may be associated with the oil used in the vacuum pump attached to our ballistic compressor. Melanophlogite is known to be unstable at high temperatures of around 1000°C and above, and breaks down invariably to cristobalite after a few days at this temperature. Therefore, if the argon gas temperature was higher in our observation, the end product may have been beta-cristobalite.

If hydrogen is mixed with argon in the ballistic compressor, we may observe diffusion of hydrogen in a sample used if it is trapped. A quartz crystal was exposed to argon mixed with 13% of hydrogen by volume. The peak conditions of the gas compression were 510 atmospheres and 2000 K. The quartz exposed to this gas was observed for hydrogen concentration as a function of depth by means of the nuclear reaction analysis technique (Fig. 4). This figure shows a near surface hydrogen concentration corresponding to SiOH with a typical diffusion profile,

$$\text{Hydrogen concentration} = A\left(1 - \frac{2}{\sqrt{\pi}} \int_0^{x/\sqrt{4Dt}} e^{-u^2} du\right), \tag{7}$$

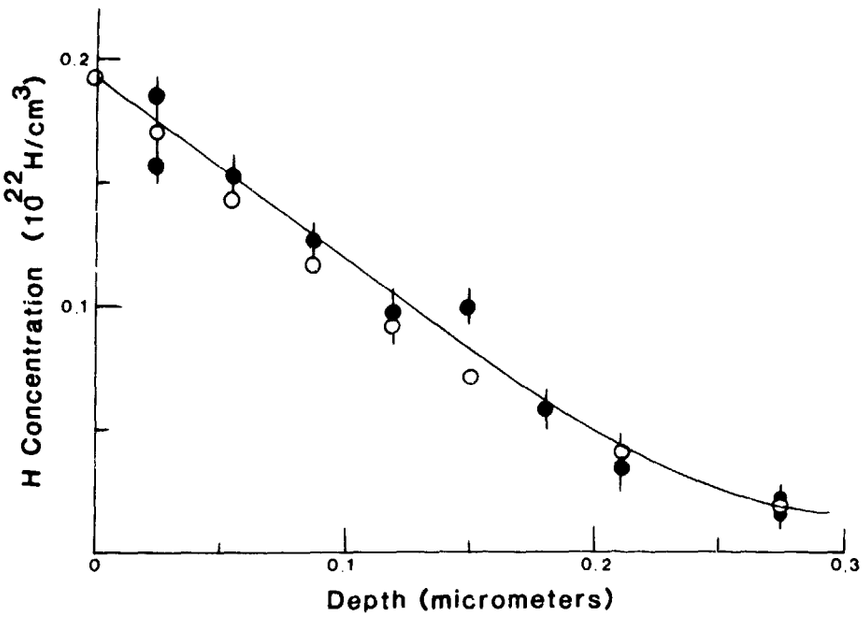

FIG. 4 *Hydrogen diffusion in quartz during exposure to argon-hydrogen mixture at 510 atmospheres and 2000 K. Black circles correspond to experimental observations. Open circles are calculated by using Eq. (7).*

where x is the depth from the quartz surface, D the diffusion coefficient which is assumed to be a constant, and t is a typical time for diffusion. In order for the concentration to behave as in Fig. 4, hydrogen must be frozen in the quartz in typical time t, and the frozen state is stable at temperatures lower than the temperature at t. Therefore, we may have a model for the hydrogen behavior as follows. Hydrogen diffuses into quartz, more or less freely during exposure to the hot, dense gas, in the form of H_2 and is trapped on cooling as SiOH, the concentration of which is nearly proportional to hydrogen concentration (more exactly with Langmuir's isotherm dependence) and which is stable at lower temperatures. Untrapped hydrogen will diffuse out as time goes on. From Fig. 4, if we choose t as about 1 millisecond, then D = 10 x 10^{-8} cm^2/sec. This value of the diffusion coefficient is comparable to that of 19 x 10^{-8} cm^2/sec for molecular H_2 in a fused silica at 1000°C [8].

An interesting observation with quartz exposed to a hot, dense hydrogen-argon mixture is that it initially glowed an orange color on bombardment with 6.5 Mev nitrogen ions, but with increasing time of

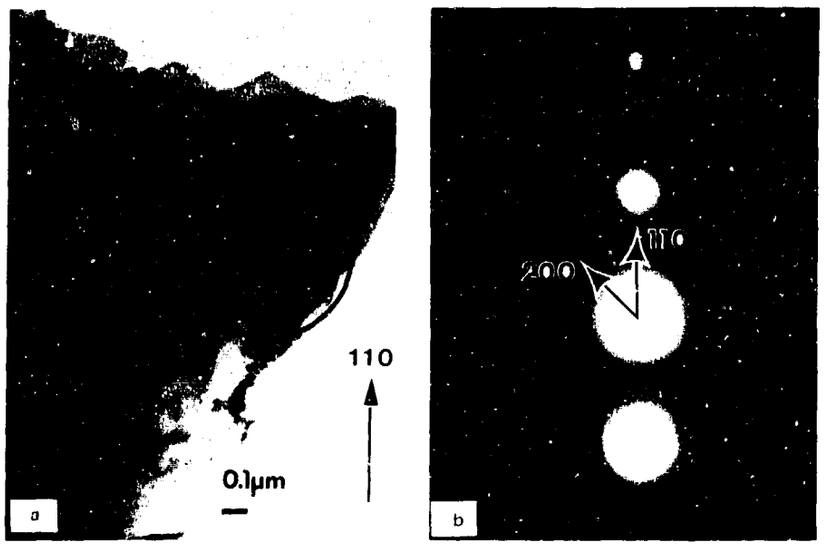

FIG. 5 *Instability of microstructure and crystal structure of iron exposed to argon-hydrogen mixture at 233 atmospheres and 1800 K. (a) and (b) Electron micrograph and electron diffraction pattern, respectively, immediately after exposure, (c) and (d) After exposure to a .05A/cm^2 electron beam in the 125 kV TEM for 7 minutes, (e) and (f) One hour after the electron beam was turned off.*

bombardment, it began to turn the more typical blue color of quartz. The ion beam might have released the trapped hydrogen

On the other hand, hydrogen is known not to be trapped with a good stability in iron or its alloys. An amorphous iron ($Fe_{78}B_{13}Si_9$) is another example, for which hydrogen solubility is small, and did not show any interesting nuclear reaction analysis results, but it seems to chemically react with hydrogen at higher temperatures and pressures. Hydrogen diffuses into the sample and may form gaseous compounds with boron and silicon of the alloy [9], thus destroying the material. In fact, the material was more easily lost (possibly vaporized completely) in the ballistic compressor if the gas contains hydrogen.

Figure 5 illustrates the instability of microstructure and crystal structure of iron exposed to hydrogen-argon mixture. Figures 5a and b are an electron micrograph and an electron diffraction pattern of iron sample immediately after exposure to a hot, dense 24% mixture at 233 atmospheres and 1800 K. They changed to those shown by Figs. 5c and d after this sample was exposed to the electron beam (current density .05A/cm^2) in the

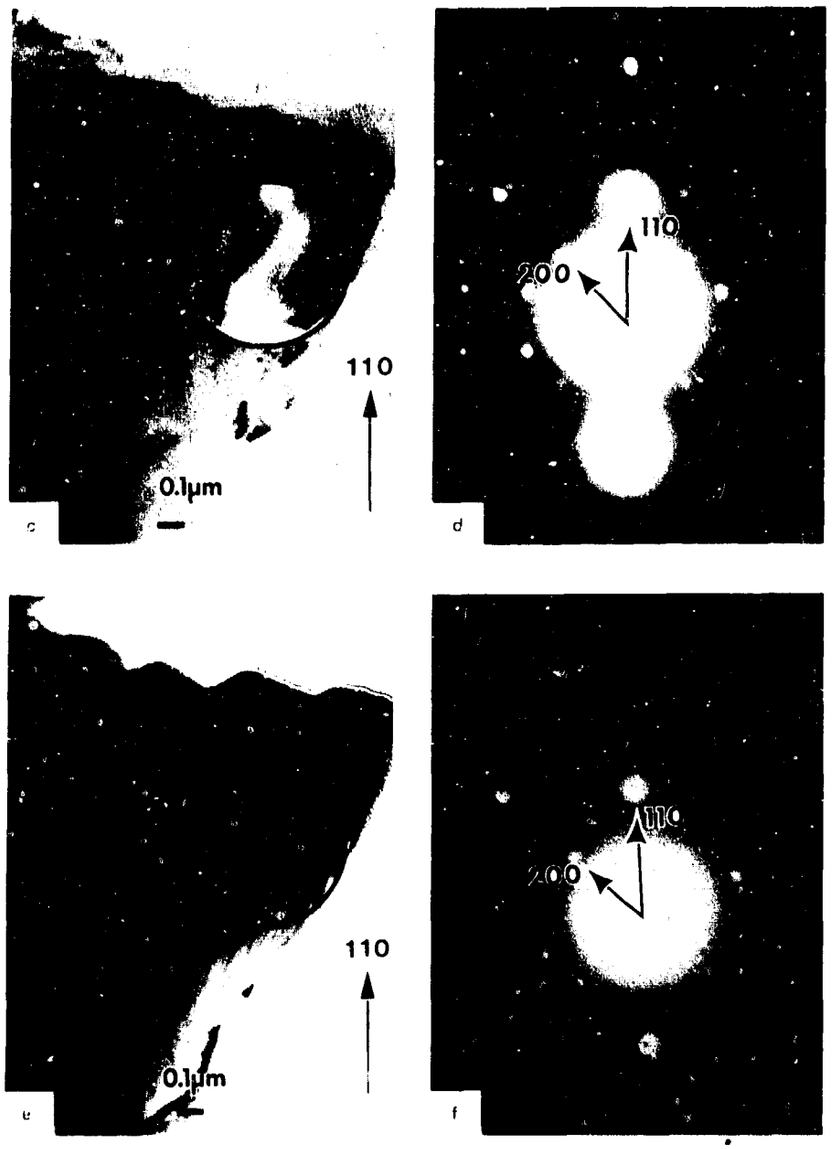

125 kV TEM for 7 minutes. Then it was left in the TEM (beam off) for one hour before Figs. 5e and f were taken. Since such drastic change must be expected at least with iron exposed to hydrogen, examination of the exposed sample must be made immediately following the exposure.

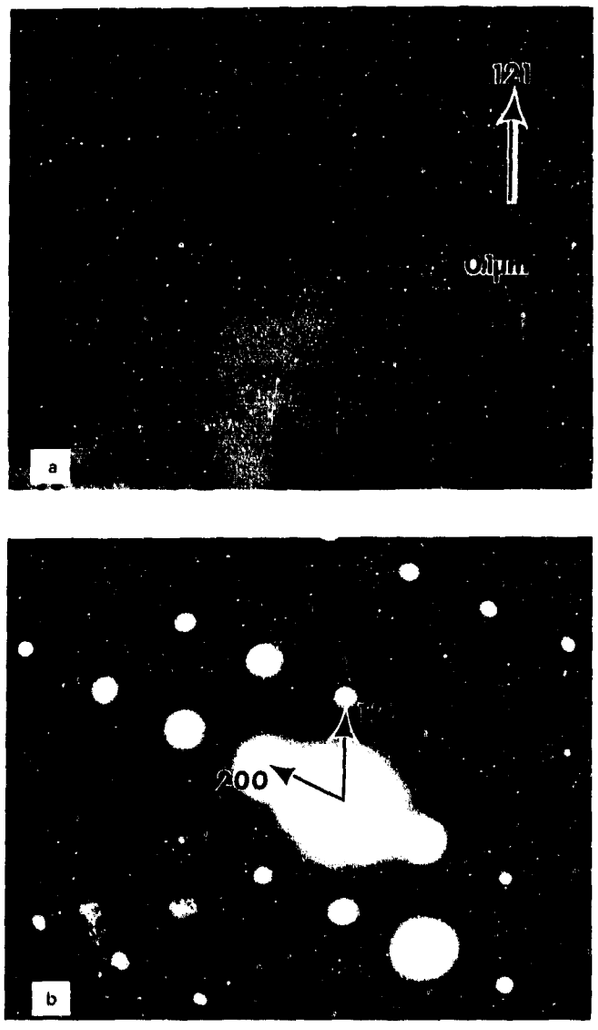

FIG. 6 *(a) Electron micrograph of 1μm thick iron foil exposed to argon-hydrogen mixture at 172 atmospheres and 1800 K, (b) Electron diffraction pattern at the circled area of (a), (c) Electron micrograph of the control, (d) Electron diffraction pattern at the circled area of (c).*

It is not likely that a high energy electron microscope may damage an unstable iron sample with hydrogen. This illustrated in Figs. oa and b, which were taken by using the 1.5 MV Berkeley TEM. The sample is a rolled and annealed iron foil (about 1 μm thick) in a folded molybdenum grid. First it was exposed to a 19% hydrogen-argon at 50 atmospheres and 1500 K.

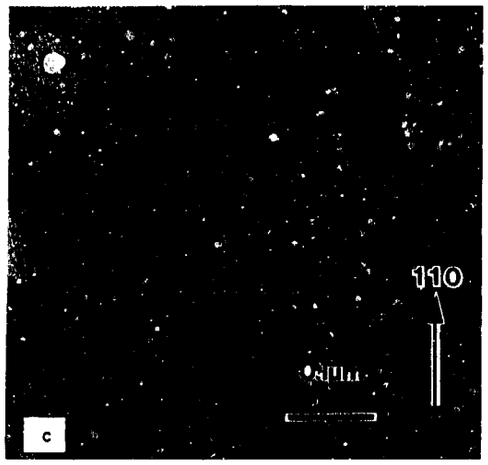

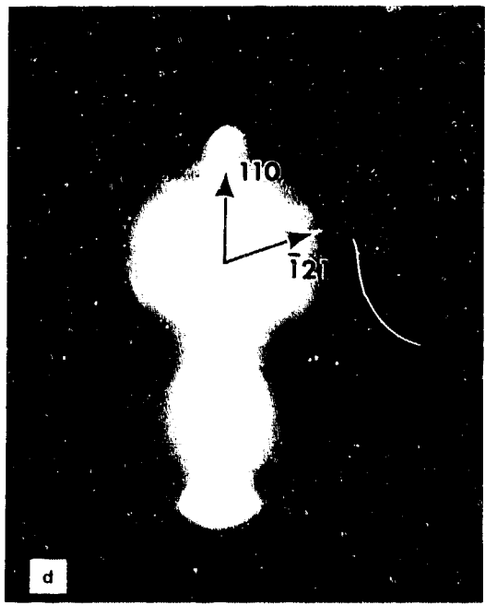

A visual observation showed no change. Next it was exposed to a 24% mixture at 172 atmospheres and 1800 K. The diffraction analysis shows a lattice distortion as shown in Table 2. The change in the d-spacing qualitatively agrees with Wallace's result [10]. The large change in d-spacing for plane (310) suggests from Wallace's result that (110) and (220) may also be associated with large strain. Such low symmetry of distortion is

TABLE 2 *Lattice strain Δ/d obtained from Fig. 7.*

Plane	(200)	(211)	(310)	(321)	(400)	(431)	(521)	(442) (600)	(532)
Δ/d	0.0	0.01	0.03	0.02	0.01	0.01	0.01	0.0	0.01

related to a uniaxially ordered crystal structure. Figure 6c is an electron micrograph of the control iron. The origin of the striations in the figure is not known.

Compared to hydrogen behavior, argon seems to behave much more simply. Figure 7 shows x-ray diffraction patterns of amorphous iron. Figure 7b shows the pattern of the material exposed to argon at 315 atmospheres and 2000 K, while Fig. 7a corresponds to that heated in argon at 1 atmosphere and 960 K. The difference in the diffraction angle (2θ) of diffraction peaks indicate the difference in the lattice parameters by about 1%. Argon seems to diffuse into the material to expand the crystal, but the details are not clear.

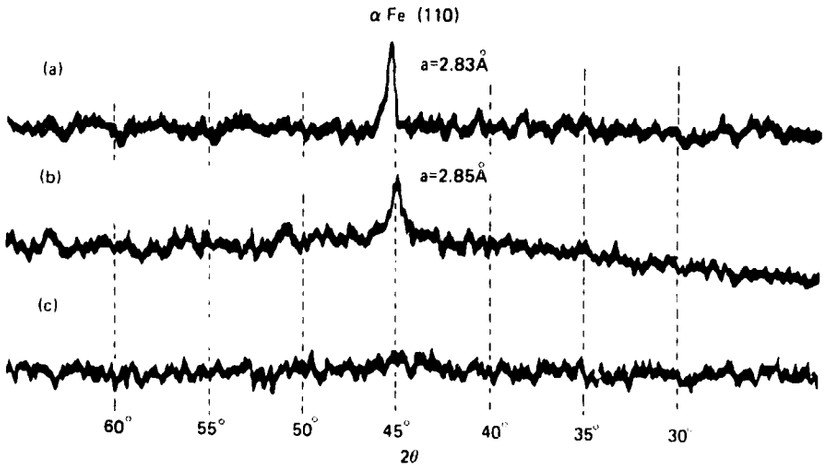

FIG. 7 *X ray diffraction patterns of amorphous iron alloy. (a) Heated in argon, (b) Exposed to argon in the ballistic compressor.*

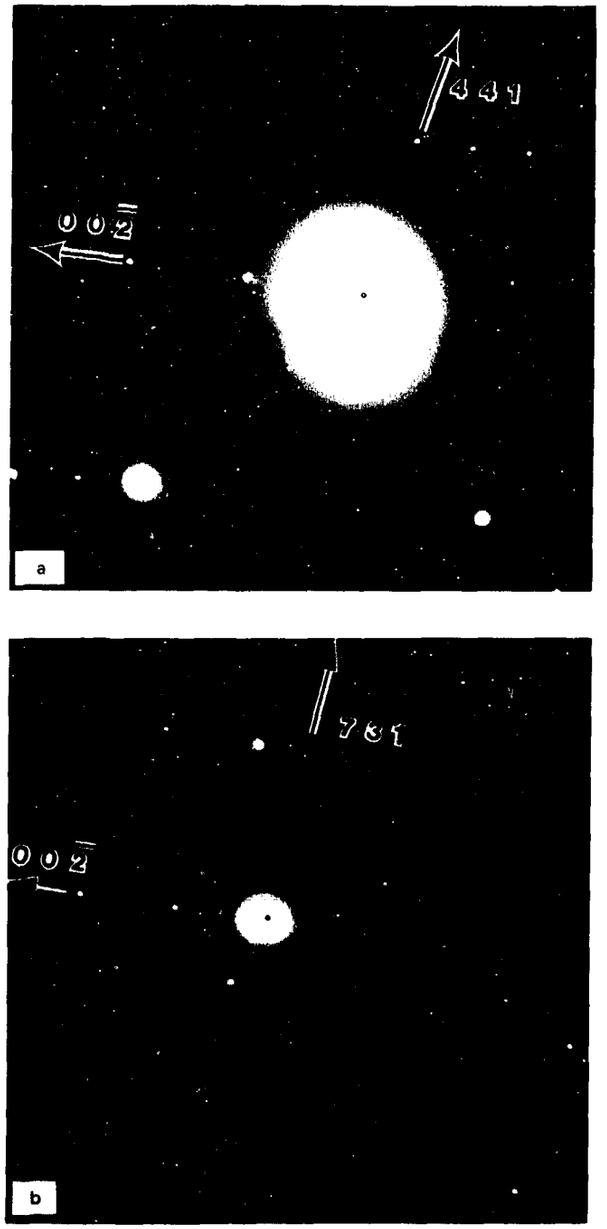

FIG. 8 *Electron diffraction patterns and micrograph of stainless steel exposed to argon at 300 atmospheres and 1800 K. (a) and (b) Diffraction patterns from particles at the corresponding symbols, a and b, in micrograph (c).*

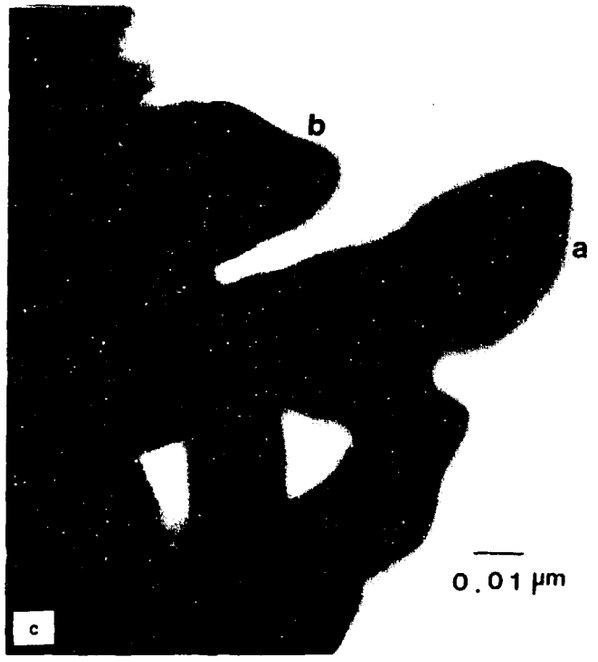

FIG. 8 *Continued.*

Not only are there changes in the lattice parameter, but also the concentration ratio of elements in alloys seems to change by exposure to hot, dense argon. The weight fractions of stainless steel (Fe18Cr12Ni) are respectively about 0.65, 0.23 and 0.11 after exposure to argon (300 atmospheres and 1800 K) compared to those of 0.70, 0.17 and 0.13 before exposure. The ratio Cr/Fe changes by 30%. The resulting microstructure and electron diffraction patterns from two individual particles in the microstructure are shown in Fig. 8. These particles have different morphology and different crystal structure than martensite formed in the normal Fe18Cr12Ni alloy by cooling to liquid nitrogen temperature [6]. The indexing shown in the patterns is consistent with the chi phase in chromium nickel steel which has body-centered cubic structure with lattice parameter 8.89Å [11].

V. ACKNOWLEDGEMENT

This research is supported by the Army Research Office. We are very grateful to D. Ackland for assistance with the 1.5 MV TEM at the National Center for Electron Microscopy, Lawrence Berkeley Laboratory. We also owe H. Karamon, Sony Magnetic Products Inc., Japan for supplying us with an amorphous iron alloy.

REFERENCES

1. W.A. Lanford and M.J. Rand, *J. Appl. Phys. 49*:2473 (1978).
2. M. Takeo, O.A. Holmes and S.Y. Ch'en, *J. Appl. Phys. 38*:3544 (1967).
3. D.E. Sterrit, G.T. Lalos and R.T. Schneider, *Special Report, University of Florida, to NASA (NGL-10-089)*, March (1973); G.T. Lalos and G.L. Hammond, *Experimental Thermodynamics of Non-Reacting Fluids*, Ch. 25, 1193-1218 (1975).
4. M. Takeo, *Bull. Am. Phys. Soc. 9*:712 (1964).
5. S.Y. Ch'en, *University of Oregon*, Private communication (1976).
6. J. Dash and H.M. Otte, *Acta Met. 11*:1169 (1963).
7. Brian J. Skinner and Daniel E. Appleman, *The American Mineralogist 48*:854 (1963).
8. *Diffusion Data Book*, Diffusion Information Center, Cleveland, Ohio, Vol. 2, 52 (1968).
9. Sin-Shong Lin, *Army Materials and Mechanics Research Center, Watertown, MA*, private communication (1985).
10. John P. Wallace, *Scripta Met. 12*:571 (1978).
11. P.K. Koh, *J. Metals, 5*:339 (1953).

A2

Review of Scientific Instruments, March 1988.

Electronic device for the analysis of electron diffraction patterns

A. Trzynka and M. Takeo

Department of Physics and Environmental Sciences and Resources, Portland State University, P.O. Box 751, Portland, Oregon 97207

(Received 22 October 1987; accepted for publication 30 November 1987)

Using a video camera, a video digitizer, and a microcomputer, an image processing system is assembled to determine the locations of electron diffraction spots on photographic negatives of electron diffraction patterns. This system can help to reduce the measurement time to one third when compared with conventional manual methods and produces results with better accuracy and less operator fatigue.

INTRODUCTION

Much work has been done on various image processing devices, and the technique on noise reduction and image contrast has been well developed.[1–6] This paper reports the construction of a new device that can make the analysis of electron diffraction patterns easier and more accurate. The conventional method of analyzing electron diffraction patterns with a micrometer positioned microscope or with divider and scale is very tedious and time consuming. It is also a possible source of human bias. Yet it provides poor precision. In general, x-ray diffraction equipment gives more precise crystallographic data than electron diffraction equipment. However, the equipment requires a large sample size since the x-ray beam cannot be made very small. Our studies involve small precipitates whose linear size is of the order of 1000 Å. Electron diffraction equipment allows us to locate a precipitate and then collect an electron diffraction pattern from the precipitate.

I. DETAILS OF CONSTRUCTION

In order to measure electron diffraction patterns with this system we need to recognize the diffraction spots as regions of maximum photographic density on the film negative of the electron diffraction pattern. We collect a video image of the electron diffraction film negative using an RS-170 standard video camera[7] and a light table. The RS 170 video standard defines the format in which the information making up video images are transmitted to the video display device such as a video monitor. The video monitor is simply a phosphor screen which is scanned by an electron beam. The electron beam current determines the displayed image brightness. The video camera is essentially the reverse of the monitor where the phosphor screen is replaced by a light-sensitive screen and an electron beam scans the light-sensitive screen. The electron beam current in the camera is dependent on the point-to-point intensity of a focused optical image on the light-sensitive screen. Essentially the RS-170 format specifies a complete image to be made up of two groups of 240 horizontal scan lines interlaced with each other and each group of 240 scan lines to be completed in $\frac{1}{60}$ s. So one complete video image (or frame) of 480 scan lines is displayed on a video monitor or collected by a video camera in $\frac{1}{30}$ s. The RS-170 video signal produced by the camera is an analog electrical signal whose amplitude determines the electron beam current in the video monitor. The RS-170 video signal also contains some important syncronizing pulses to allow housekeeping tasks such as electron beam blanking and retrace. We sample the amplitude of the RS-170 video signal and convert it to digital form by a high-speed 8-bit analog-to-digital converter as it comes from the camera and write the digital information to an array of random access memory called the frame memory. We can sample and digitize the RS-170 video signal either continuously frame after frame with continuous rewriting of the digital information to the frame memory, or we can sample, digitize, and write one video frame of 480 horizontal scan lines to the frame memory, and then stop further sampling, digitizing, and writing to the frame memory until more data are desired. The sample and digitizing rate is 512 times per horizontal scan line. The frame memory is organized as a two-dimensional array of memory cells with each cell containing the digital value written to it as the RS-170 video signal was sampled and digitized. The digital values contained in the frame memory are positive integers and are commonly called "pixels" or PICture ELements. The frame memory is large enough to store one complete video frame as 512 pixels horizontally by 480 pixels vertically. The pixels are continuously read from the frame memory to a digital-to-analog converter and after the necessary syncronizing pulses are added to meet the requirements of the RS-170 format the contents of the frame memory are displayed on the video monitor. The frame memory can be read from or written to by a microcomputer, and thus image processing operations can be performed on the image. A block diagram of our system is given in Fig. 1.

We prefer to work with a positive image displayed on the video monitor rather than the negative film image be-

cause with a positive image the electron diffraction spots can then be recognized as groups of pixels whose values are greater than the background pixels. Since we can read from and write to any of the frame memory locations with the microcomputer, we can invert the complete image by logically inverting (1000 1101 binary is changed to 0111 0010 binary) every pixel in the frame memory. The inversion process results in the frame memory being filled with positive digital representation of the electron diffraction pattern and a positive image of the electron diffraction film negative displayed on a video monitor. The electron diffraction spots are now represented as groups of pixels whose digital values are

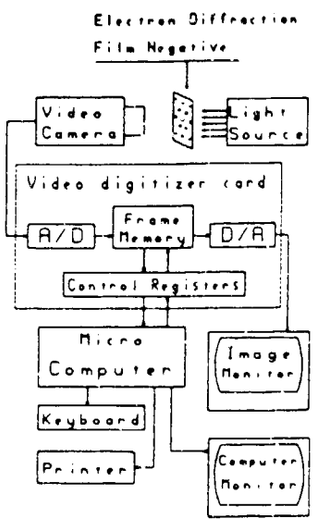

FIG. 1. Block diagram of image processing system.

greater than the surrounding pixels. Since we can read from the frame memory with the microcomputer, we can search the frame memory for the greatest value pixels. As we perform this search we know the location in the frame memory of each pixel we are examining. If we convert the frame memory locations of the greatest value pixels to real locations on the negative, then we will have determined the locations of the electron diffraction spots and "measured" the electron diffraction pattern.

The video camera used to collect the electron diffraction image should produce an image as noise free as possible since after sampling and digitization, any noise peaks in the frame memory will be interpreted as false electron diffraction spots. The main source of noise is the photosensitive element of the video camera where thermal noise is generated. Since the thermal noise is random we can reduce this noise by averaging many images which differ only in random noise. By averaging images we mean adding together the digital values at each pixel location for all images then dividing every pixel value in the resultant image by the number of images summed. The summing of images is a process carried out by the microcomputer. The resulting average image is then transferred to the frame memory. In our testing we found that vidicon tube cameras generate greater image noise than charge-coupled device (CCD) video cameras. We will discuss the differences in video camera performance later.

To make accurate measurements of the image, we must correct for the rectilinear distortion introduced by the video camera and lens system. We correct for rectilinear distortion and make the conversion from frame memory pixel coordinates to real-space coordinates by comparing the digitized electron diffraction film negative image with the digitized image of a specially made calibration standard. The calibration standard is an accurately formed square array of dots located 0.500 cm apart on a plane surface slightly larger than the electron diffraction film negatives we wish to process. A table of data-correlating frame memory pixel corrdinates with the real-space coordinates as defined by the calibration standard is created each time the camera position or lenses are changed and we are then able to refer to this table of data when we wish to convert frame memory pixel coordinates to real-space coordinates. Two-dimensional linear interpolation is performed when the frame memory pixel coordinates we wish to convert to real-space coordinates are not found directly in the table. The microcomputer is programmed to do the messy work of creating the table of data from the calibration standard image and the conversion of the frame memory pixel coordinates to real-space coordinates.

We determine the frame memory pixel coordinates of an electron diffraction spot by first defining, by means of an operator-positionable cursor, an area within the displayed image which contains a single electron diffraction spot of interest. Defining an area within the image serves five purposes: (1) The operator is able to measure only those spots of interest. (2) The defined area contains only one electron diffraction spot, so there will be only one group of pixels in the defined area which are greater than all others within the defined area. (3) Defining an area within the displayed image specifies the portion of the frame memory that contains the digital data for the defined area. (4) If the area defined is made as small as possible, processing time will be reduced. (5) The defined area helps the operator keep track of which electron diffraction spots have been processed.

After defining an area containing one electron diffraction spot we apply a low-pass spatial filter to the defined area to "smooth" the portion of the image within the defined area. This low-pass spatial filter process is essentially a two-dimensional moving average. The low-pass spatial filter will tend to remove isolated single-pixel peak values from the defined area by averaging groups of nine pixels to find the average pixel value for each group. We use a group size of nine pixels (the pixel to be processed and its eight nearest neighbors) with every pixel in the group equally weighted. The low-pass spatial filter is a software process implemented by the microcomputer and applied to all the pixels within the operator-defined area. The low-pass spatial filter will re-

move some of the random noise generated by the video camera, but we choose to perform the image averaging and scaling of the whole image, saving the low-pass spatial filter step for the operator-defined areas, since the low-pass spatial filter is a computationally intense process and is comparatively slow when applied to large image areas. Following the low-pass filtering, the microcomputer examines the digital values of all the pixels within the defined region of frame memory for the maximum value pixels and then averages the frame memory coordinates of these maximum value pixels to find a single pair of frame memory coordinates that most probably describe the location of the electron diffraction spot. Next the microcomputer performs the frame memory pixel coordinate to real-space coordinate conversion and allows the operator to write the data to a disk file for storage and later processing.

II. EXPERIMENTAL RESULTS

We chose a typical electron diffraction film negative and measured it repeatedly with our system using both a vidicon tube video camera and a CCD video camera. Using our tube video camera we were able to take spatial measurements of the electron diffraction spots containing an uncertainty of $\pm$ 0.0052 times the image width with 99% confidence limits (after summing 16 images to reduce random noise). The CCD video camera allows us to take the same measurements but with an uncertainty of $\pm$ 0.0018 times the image width with 99% confidence limits (after summing 16 images to reduce random noise). The CCD video camera produces results with an uncertainty near one third that of the tube video camera (after summing 16 images for both cameras) when tested using the same procedure. Table I contains the uncertainties for both cameras when different numbers of images are summed to reduce the random noise and Fig. 2 is a plot of this data. The following procedure was used to determine the listed uncertainty. Take row three of Table I as an example: Five different images of the same diffraction pattern were compiled, each of the five images being the average of 16 previously collected images which differed only in random noise content. For each of the five compiled images, 15 distances were measured using this system and the standard deviation for each distance calculated. The standard deviation is corrected for the small sample size of five by use of the "Student's t" for 99% confidence limits, thus giving the 15 measurements with their uncertainties at the 99% confidence limit. The uncertainties for the 15 measurements are then averaged and listed under the appropriate heading for the camera type (16 images summed, uncertainty of 0.009 cm for the CCD camera, uncertainty of 0.026 cm for the tube camera). It is interesting to note that with increasing quantities of images averaged to form the compiled image the uncertainty decreases and reaches a minimum at near 16 images but is then found to increase again. This increase in the uncertainty is thought to be due to camera vibration.

TABLE I. Uncertainty in results obtained after summing various numbers of images.

Images summed	Uncertainty (cm)	
	CCD	Tube
1	0.016	0.053
4	0.011	0.049
16	0.009	0.026
64	0.016	0.040
125	0.012	0.040

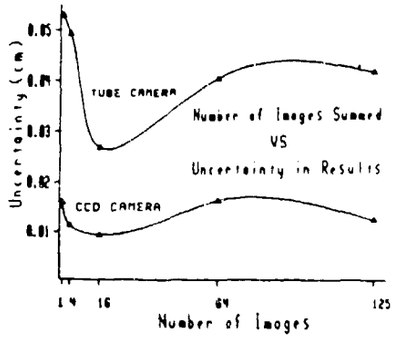

FIG. 2. Plot of data contained in Table I.

Figure 3 is an electron diffraction pattern of BCC iron and Table II is a compilation of the data output from this system after processing this electron diffraction pattern. The spot numbers in Table II correspond to the numbered spots in Fig. 3. The large percent error in distance (greater than about 1%) associated with spot numbers two and six relative to predicted values can be explained as these spots are actually double spots of similar photographic density (revealed by careful examination of the negative) caused by some defect in the crystal structure of the iron sample. These double spots are too close together to be measured as individual spots when the negative is imaged at suitable magnification to include all the remaining spots of interest.

III. EQUIPMENT

The video camera we use is a model WV-CD50 manufactured by Panasonic Industrial Company. This is a CCD-type video camera incorporating a silicon detector containing 510 light-sensitive cells horizontally and 492 light-sensitive cells vertically. The video digitizer we use is a PCVISION FRAME GRABBER manufactured by Imag-

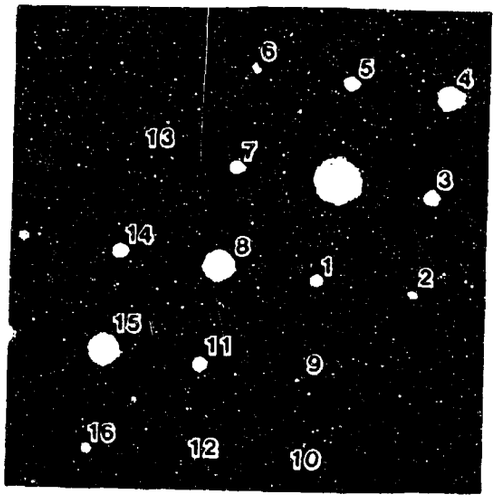

FIG. 3. Electron diffraction pattern of BCC iron. ([001] zone axis.)

TABLE II. Data after processing of the electron diffraction pattern pictures in Fig. 3.

Spot number	hkl	Distance (cm) Exp	Predict	% error	Angle (deg) Exp	Predict	Error
1	110	1.195	1.195	0.0	0.0	0.0	0.0
2	200	1.649	1.690	2.43	45.0	45.0	0.0
3	$1\bar{1}0$	1.202	1.195	0.58	90.3	90.0	0.3
4	$0\bar{2}0$	1.702	1.690	0.71	134.7	135.0	0.3
5	$\bar{1}\bar{1}0$	1.201	1.195	0.50	179.7	180.0	0.3
6	$\bar{2}00$	1.658	1.690	1.89	225.1	225.0	0.1
7	$\bar{1}10$	1.203	1.195	0.67	270.1	270.0	0.1
8	020	1.710	1.690	1.18	315.1	315.0	0.1
9	220	2.371	2.390	0.79	359.1	360.0	0.9
10	330	3.552	3.586	0.95	359.3	360.0	0.7
11	130	2.684	2.673	0.41	333.3	333.4	0.1
12	240	3.780	3.780	0.0	341.1	341.6	0.5
13	$\bar{2}20$	2.389	2.390	0.04	270.5	270.0	0.5
14	$\bar{1}30$	2.690	2.673	0.64	296.7	296.6	0.3
15	040	3.418	3.381	1.09	315.0	315.0	0.0
16	150	4.330	4.310	0.46	326.2	326.3	0.1

ing Technology Incorporated. This video digitizer has a spatial resolution of 512×480 pixels and a dynamic range of 8 bits per pixel. The spatial resolution of 512×480 pixels is limited by the RS-170 standard video signal format. To increase the spatial resolution will require a special high-resolution video camera and video digitizer with their corresponding increase in cost. We felt that 1% accuracy was a reasonable goal when planning this system. The size of the diffraction pattern on our negatives is typically 5×5 cm and to make the math simple, lets say 5.12×4.8 cm. If this region is sampled and digitized with a spatial resolution of 512×480 pixels then each pixel is 0.01 cm on its side, thus the distance between two diffraction spots separated by 1 cm could be measured with an accuracy of 1%. This system can take measurements containing an uncertainty of ± 0.0018 times the image width with 99% confidence or as in the above example: ~~5.12 cm~~ $\pm 0.0018 = \pm 0.0092$ cm at the 99% confidence level or about 1%. The dynamic range is actually 7 bits per pixel since we use 1 bit of the eight as an overlay on the diffraction pattern image to provide information to the operator. A Zenith model 158 microcomputer serves as the host for the video digitizer. The image summing process used to reduce random noise by averaging images requires that the microcomputer contain 640 kbytes of random access memory. The Zenith model 158 includes a 20-Mbyte hard-disk drive which is very useful when saving images since a single image will take about 256 kbytes of disk space. Two video monitors display information in our system. The microcomputer monitor displays only text, while the second monitor is a small monochrome one that displays the image being processed. A dot-matrix printer is used to print the data and images processed.

The use of a film negative to record the electron diffraction pattern imposes some contrast limitations on the entire electron diffraction pattern because of the narrow exposure latitude of the photographic film. If the video camera were installed to view the electron diffraction pattern through an electron-optical coupler in the electron microscope, the precision could possibly be improved because of increased dynamic range in image intensity and because the diffraction spots could each be adjusted for their best sharpness so long as the size and orientation of the pattern does not change. Alternatively, some form of an electron imaging device could prove useful since the electron-optical coupling could then be eliminated. The use of a film negative, however, provides a stable record of the electron diffraction pattern and the opportunity to use film negatives from other electron mircoscopes.

ACKNOWLEDGMENTS

Walt Skoczylas and Gert Rempfer of Portland State University gave useful hardware recommendations. Wister Macomson gave useful programming recommendations. This is Portland State University Environmental Sciences and Resources Program Publication No. 220. This research is supported by the U.S. Army Research Office.

[1] John F. Asmus, Byte, 12, 151 (1987)
[2] Gregory A. Baxes, *Digital Image Processing* (Prentice-Hall, Englewood Cliffs, NJ, 1984)
[3] Benjamin M. Dawson, Byte, 11, 96 (1986)
[4] Benjamin M. Dawson, Byte, 12, 169 (1987)
[5] Charles McManis, Byte, Vol. 12, 191 (1987)
[6] Ken Sheldon, Byte, 12, 143 (1987)
[7] Gerald P. McGinty, *Video Cameras: Operation and Servicing* (Howard W. Sams, Indianapolis, IN, 1984)